STEM CELLS®

REGENERATIVE MEDICINE

Alpha-Ketoglutarate Curbs Differentiation and Induces Cell Death in Mesenchymal Stromal Precursors with Mitochondrial Dysfunction

KARMVEER SINGH [a,b] LINDA KRUG,[a,b] ABHIJIT BASU,[a] PATRICK MEYER,[a,b] NICOLAI TREIBER,[a,b] SEPPE VANDER BEKEN,[a] MEINHARD WLASCHEK,[a,b] STEFAN KOCHANEK,[c] WILHELM BLOCH,[d] HARTMUT GEIGER,[a,b,e,f] PALLAB MAITY,[a,b] KARIN SCHARFFETTER-KOCHANEK[a,b]

Key Words. Aging • Differentiation • Epigenetics • Mesenchymal stem cells • Multipotential differentiation • Osteoporosis • Plasticity • Hypoxia

ABSTRACT

Increased concentrations of reactive oxygen species (ROS) originating from dysfunctional mitochondria contribute to diverse aging-related degenerative disorders. But so far little is known about the impact of distinct ROS on metabolism and fate of stromal precursor cells. Here, we demonstrate that an increase in superoxide anion radicals due to superoxide dismutase 2 (Sod2) deficiency in stromal precursor cells suppress osteogenic and adipogenic differentiation through fundamental changes in the global metabolite landscape. Our data identify impairment of the pyruvate and L-glutamine metabolism causing toxic accumulation of alpha-ketoglutarate in the *Sod2*-deficient and intrinsically aged stromal precursor cells as a major cause for their reduced lineage differentiation. Alpha-ketoglutarate accumulation led to enhanced nucleocytoplasmic vacuolation and chromatin condensation-mediated cell death in *Sod2*-deficient stromal precursor cells as a consequence of DNA damage, Hif-1α instability, and reduced histone H3 (Lys27) acetylation. These findings hold promise for prevention and treatment of mitochondrial disorders commonly associated with aged individuals. STEM CELLS *2017;35:1704–1718*

SIGNIFICANCE STATEMENT

We identified a profound metabolite imbalance in the superoxide dismutase 2-deficient stromal precursors with faulty mitochondria affecting both glycolytic and oxidative metabolism, which subsequently impairs differentiation process. These findings hold promise for prevention and treatment of mitochondrial disorders commonly associated with aged individuals.

[a]Department of Dermatology and Allergic Diseases, [b]Aging Research Center (ARC), Ulm, Germany; [c]Department of Gene Therapy, [d]German Sport University Cologne, Germany; and [e]Institute of Molecular Medicine and Stem Cell Aging, University of Ulm, Ulm, Germany; [f]Division of Experimental Hematology and Cancer Biology, Cincinnati Children's Hospital Medical Center and University of Cincinnati, Cincinnati, Ohio, USA

Correspondence: Karin Scharffetter-Kochanek, M.D., Department of Dermatology and Allergic Diseases, University of Ulm, Albert-Einstein-Allee 23, 89081 Ulm, Germany. Telephone: 49-731-5005-7501; Fax: 49-731-5005-7502; e-mail: karin.scharffetter-kochanek@uniklinik-ulm.de; or Pallab Maity, Department of Dermatology and Allergic Diseases, University of Ulm, Albert-Einstein-Allee 23, 89081 Ulm, Germany. Telephone: 49-731-5005-7661; Fax: 49-731-5005-7660; e-mail: pallab.maity@uni-ulm.de

Received November 9, 2016; accepted for publication March 28, 2017; first published online in STEM CELLS *EXPRESS* April 11, 2017.

1066-5099/2017/$30.00/0

http://dx.doi.org/10.1002/stem.2629

INTRODUCTION

Metabolic pathways, including glycolysis, tricarboxylic acid (TCA) cycle, and beta-oxidation, play a pivotal role in the biosynthesis of distinct electron donors, which fuel the mitochondrial respiratory chain to generate energy [1]. Mitochondrial dysfunction interrupts this highly regulated process resulting in diverse pathologies such as cancer, cardiomyopathy, metabolic, and degenerative disorders, and aging [2, 3]. A progressive age-dependent decline in oxidative phosphorylation (OXPHOS) efficiency and mtDNA content further support this notion [4]. However, the molecular mechanisms linking mitochondrial dysfunction to specific symptoms and pathologies are largely unexplored.

Under normal conditions, mitochondrial antioxidant enzyme manganese superoxide dismutase (MnSOD or Sod2) constantly scavenge superoxide anion radicals ($O_2^{\bullet-}$) generated during respiration and thus ensures normal growth and development. Dysfunctional Sod2 has been associated with cardiomyopathy, cancer, neurodegenerative diseases, and several aging phenotypes [5–8].

Recently, the focus has shifted to better understand the contribution of biosynthetic functions of mitochondria in normal physiology and pathological conditions [9, 10]. Interestingly, high-energy mitochondrial metabolic products, such as acetyl-coA, succinate, and α-ketoglutarate, were suggested to directly influence the epigenome through post-translational modifications of histones, DNA, and transcription factors [11] referred to as "metabolic reprogramming."

Compelling evidence suggested an involvement of distinct mitochondrial-derived reactive oxygen species (ROS), such as superoxide anions ($O_2^{\bullet-}$) in the metabolic shift toward aerobic glycolysis and most likely in "metabolic reprogramming" [12–14]. However, detailed knowledge on metabolite diversity and consequences of this metabolic

adaptation on tissue homeostasis with respect to differentiating stromal precursor cells is largely lacking. Stem cells and progenitors cells, irrespective of their histogenetic background and tissue location, undergo dramatic changes with increased mitochondrial biogenesis and subsequent oxidative metabolism essentially required for lineage differentiation [15, 16]. Using specific biochemical and genetic approaches, we wished to investigate metabolic changes in mesenchymal stromal precursor cells in response to enhanced mitochondrial $O_2^{\bullet-}$ concentrations. For this purpose, we used stromal precursor cells isolated from the stroma specific *Sod2*-deficient premature aging model. This model—due to enhanced concentrations of $O_2^{\bullet-}$ and mitochondrial dysfunction—closely recapitulate intrinsic aging and related aging phenotype like osteoporosis, sarcopenia, and skin atrophy [7]. Here, we set out to explore whether metabolic shift in response to high concentrations of mitochondrial ROS affects cellular homeostasis and function, in particular, the differentiation potential of stromal precursor cells.

Materials and Methods

Isolation and Culture of Murine Skin Stromal Precursors

Skin stromal precursors were isolated from new born control (co) and stroma-specific *Sod2*-deficient mice (mut) by performing collagenase digestion. Skin stromal precursors were easily distinguished from other resident cells due to their adherent properties. Primary mouse skin stromal precursors were further characterized by the presence of distinct surface markers [17]. These stromal precursors were cultured in Dulbecco's modified Eagle's medium (25 mM D-glucose, 4 mM L-glutamine [L-Glut], and no sodium pyruvate [SP]) supplemented with 10% fetal bovine serum, penicillin (100 U/mL), and streptomycin (50μg/mL) under 3% and 21% O_2 tension. In case of aging studies, skin stromal precursors were isolated either from young (3 weeks) or old (90 weeks) mice in similar manner and subjected directly to the metabolomics experiments and lineage differentiation assays.

In Vitro Adipogenic, Osteogenic, and Chondrogenic Differentiation Assay

Adipogenic, osteogenic, and chondrogenic differentiation assay were performed according to manufacturer's (Lonza, Cologne, Germany, http://www.lonza.com/about-lonza/company-profile/locations-worldwide/cologne-germany.aspx) protocol. After 21 days, the adipocytes were stained with oil red O while alizarin red staining was used to detect osteocytes. For quantification, absorbance of extracted dyes were measured at 492 nm and 405 nm, respectively, for oil red O and alizarin red. H&E staining was used to detect differentiated chondrocytes.

Western Blot Analyses and Immunofluorescence Staining

Western blot analyses and immunofluorescence staining were performed as described previously [18].

Electron Microscopy

Electron microscopy was performed as described previously [7].

Measurement of MMP and ROS by Fluorescence-Activated Cell Sorting

For JC-1, dihydroethidium (DHE), and CM-H_2DCFDA experiments, cells were cultured under glycolytic or enforced oxidative conditions for 48 hours before the addition of 5,5′,6,6′-tetrachloro-1,1′,3,3′-tetraethylbenzimi- dazolylcarbocyanine iodide (JC-1) (2 μM), DHE (10 μM), or CM-H_2DCFDA (1 μM) to the culture medium. Cells were incubated for an additional 20 minutes before being trypsinized and resuspended. Mean fluorescence intensities (MFIs) were measured via flow cytometry, and a minimum of 100,000 cells were counted for each sample.

Extracellular Acidification Rate and Oxygen Consumption Rate Measurements

Oxygen consumption rate (OCR) and extracellular acidification rate (ECAR) was measured by Seahorse Bio-analyzer XF^{e}96. For measurement, 20,000 cells were seeded per well in 96-well Seahorse XF plate with overnight incubation at 3% or 21% O_2 and 5% CO_2. The cells were incubated for 60 minutes in XF^{e}96 incubator in 50 μL XF assay medium containing 0 mM glucose (Seahorse Bioscience: Santa Clara, CA 95051, United States. http://www.agilent.com/en-us/promotions/xftechnologyoverview) before ECAR/OCR estimation. The assay media were replaced with 180 μL of fresh assay media containing 5 mM physiological glucose. The assay was carried with Port A, B, C, and D containing 2 μM oligomycin, blank, 0.5 μM 2-deoxyglucose, and 0.5 μM (rotenone + antimycin). For analysis, WAVE software (Seahorse Biosciences) was used. The graphical representation of the assay was performed using Graph Pad Prism Software.

Targeted Metabolite Profiling

The metabolite analysis by liquid chromatography–tandem mass spectrometry (LC-MS) was performed using a LCMS-8050 by Shimadzu triple quadrupole mass spectrometer equipped with an electrospray ionization source and operated in multiple reaction mode. The quantification and comparison of different metabolites were performed in each groups consisting 5×10^6 stromal precursors.

Gene Expression Analyses

Quantitative real-time polymerase chain reaction was performed as described previously [18].

Statistical Calculations

Error bars represent SEM. The significance of differences between two groups was analyzed by two-tailed Student's *t* test and more than two groups by one-way analysis of variance, followed by Bonferroni correction for comparing the difference between more than two groups and presented as *, $p < .05$; **, $p < .01$; or ***, $p < .001$. The heatmap, multivariate principal component analysis, volcano plot, and Venn diagram were generated using *r* scripts.

Results

Multiple Lineage Differentiation and Mitochondrial Function Is Disturbed in *Sod2*-Deficient Stromal Precursor Cells

Cellular differentiation plays an essential role in tissue function and homeostasis. To investigate how metabolic adaptation in

response to enhanced ROS concentration influence lineage differentiation, we subjected control (wild type) and *Sod2*-deficient stromal precursor cells expressing characteristic surface markers (Supporting Information Fig. S1A–S1C) [17]—hereafter referred to as co and mut precursors—to differentiation induction media.

To determine whether the *Sod2* deficiency impair stromal cells differentiation, we cultured co and mut precursors in osteogenic differentiation medium for 21 days under conditions of 3% and 21% oxygen (O_2). Under low-oxygen tension (3%), we did not observe Alizarin red staining, indicative of extracellular matrix (ECM) calcification, in both co and mut precursors (Fig. 1A; Supporting Information Fig. S2A). Interestingly, at high-oxygen tension (21%), we observed a significant decrease in the deposition of ECM in mut compared with co stromal precursors, indicating a suppressive role of mitochondria lacking *Sod2* with subsequently increase in ROS on osteogenic differentiation (Fig. 1A; Supporting Information Fig. S2A).

At low-oxygen tension (3%) contrary to previous report [19], we observed significantly higher conversion of stromal precursors into mature adipocytes during a 21-day culture period in defined adipogenic differentiation induction media (Fig. 1B; Supporting Information Fig. S2B). The observed differentiation to adipogenic lineage under low-oxygen tension was even higher when compared with high-oxygen condition (Fig. 1B; Supporting Information Fig. S2B). Of note, under mild hypoxic conditions, we did not find any differences in adipogenic differentiation between co and mut precursors (Fig. 1B; Supporting Information Fig. S2B). Interestingly, at higher oxygen tension (21%), the numbers of mature adipocytes were significantly decreased in mut compared with co stromal precursors (Fig. 1B; Supporting Information Fig. S2B). These data suggest impaired adipogenic differentiation of mut precursors at higher oxygen tension. By contrast, chondrogenic differentiation was not significantly affected in mut precursors (Supporting Information Fig. S2C) although the pellet size indicative of chondrocyte mass was smaller compared with co stromal precursors. These findings can at least in part be explained by the fact that chondrogenesis largely rely on hypoxic conditions and to a lesser extent require oxidative mitochondrial metabolism for differentiation [20]. In addition, we observed diminished mitochondrial membrane potential (MMP)—a robust indicator of ATP production and mitochondrial activity—in mut precursors both at low- and high-oxygen conditions, and the magnitude was higher at 21% O_2 (Supporting Information Fig. S2D). Furthermore, a significant increase in superoxide anions ($O_2^{\bullet-}$) was detected (Supporting Information Fig. S2E), while a decrease in hydrogen peroxide concentrations was found (Supporting Information Fig. S2F) in mut precursors under both 3% oxygen and 21% oxygen culture conditions, suggesting that $O_2^{\bullet-}$ most likely drives differentiation defects in mut stromal precursor cells.

To investigate the impact of *Sod2* deficiency on mitochondrial respiration, we have evaluated the OCR (indicative of OXPHOS) through real-time flux analyzer in co and mut stromal precursor cells. Compared with co, mut precursors demonstrated decreased basal OCR at 3% oxygen and decreased maximal OCR as assessed after FCCP treatment both at 3% and 21% oxygen conditions suggesting suppression of oxidative metabolism in the mut precursors (Fig. 1C).

We next sought to determine the effect of *Sod2* deficiency on the glycolytic flux by measuring the ECAR (indicative of aerobic glycolysis). The mut precursors displayed a modest, although significant increase in ECAR both at basal and in response to glucose under 3% oxygen conditions, while a marked increase in ECAR was noticed after oligomycin-stimulation when compared with co stromal precursors (Fig. 1D). These data corroborate previously published reports [12–14], suggesting a profound glycolytic shift in response to enhanced $O_2^{\bullet-}$ concentration. Together OCR and ECAR changes in mut precursors may constitute an adaptive response to prevent further increase in $O_2^{\bullet-}$ concentrations or any other deleterious intermediates leaked out from the respiratory chain.

To address the question whether these in vitro findings have relevance in vivo, we further analyzed stromal cell (connective tissue) specific *Sod2*-deficient mice (mutant). Notably, mutant mice display typical features of severe osteoporosis such as reduced thickness of the articular cartilage, epiphyseal disk, cortical, and trabecular bones (Fig. 1E). In addition, a significant reduction in the differentiated osteocyte layer of the bone was observed in mutant mice (Fig. 1E). Similarly, the immunostaining of fatty acid binding protein 5 indicates that not only the subcutaneous fat layer but also the size of individual adipocyte was significantly decreased in mutants (Fig. 1F). In addition to reduced subcutaneous fat in the skin, we observed significantly reduction in fat mass at distinct sites such as interscapular brown adipose tissue and perigonadal white adipose tissue (Supporting Information Fig. S3A) in mutant mice, suggesting suppression of adipocyte precursor differentiation. In aggregate, these in vivo data are in line with our in vitro findings and suggest the importance of healthy mitochondria with balanced superoxide anion concentrations in tissue maintenance and homeostasis.

Increased Nucleocytoplasmic Vacuolation and Chromatin Condensation in *Sod2*-Deficient Stromal Precursors During Oxidative Metabolism

Next, we examined mut precursors under differentiation conditions for any morphological alteration that might influence their fate. Interestingly, mut precursors revealed a gradual increase in nucleocytoplasmic vacuolation and chromatin condensation when subjected to either osteogenic or adipogenic differentiation media under 21% oxygen conditions (Supporting Information Fig. 2A, 2B). These precursors depicting distorted morphology eventually undergo cell death. Cell death at the expense of lineage commitment most likely plays a major role in the differentiation failure observed in mut precursors.

Stromal progenitors when differentiating rely mainly on oxidative metabolism of glutamine and pyruvate, which constitutes the major ingredients of the induction media, for the biosynthesis of ECM or fat synthesis [20]. We, therefore, addressed the question, whether nucleocytoplasmic vacuolation and impaired differentiation found in mut precursors are linked to oxidative metabolism stimulated by glutamine and pyruvate. We cultured stromal precursors in medium rich with either glutamine (40 mM L-Glut) or pyruvate (50 mM SP) or both (40 mM L-Glut + 50 mM SP) for 24 to 48 hours under high-oxygen tension (21% O_2), in the absence of glucose (Fig. 2C). A substantial nucleocytoplasmic vacuolation and chromatin condensation was observed after 48 hours under conditions mimicking persistently increased oxidative metabolism (40 mM L-Glut + 50 mM SP, 21% O_2) (Fig. 2C), similar to what we observed during lineage differentiation (Fig. 2A, 2B). The number of cells displaying both nuclear and

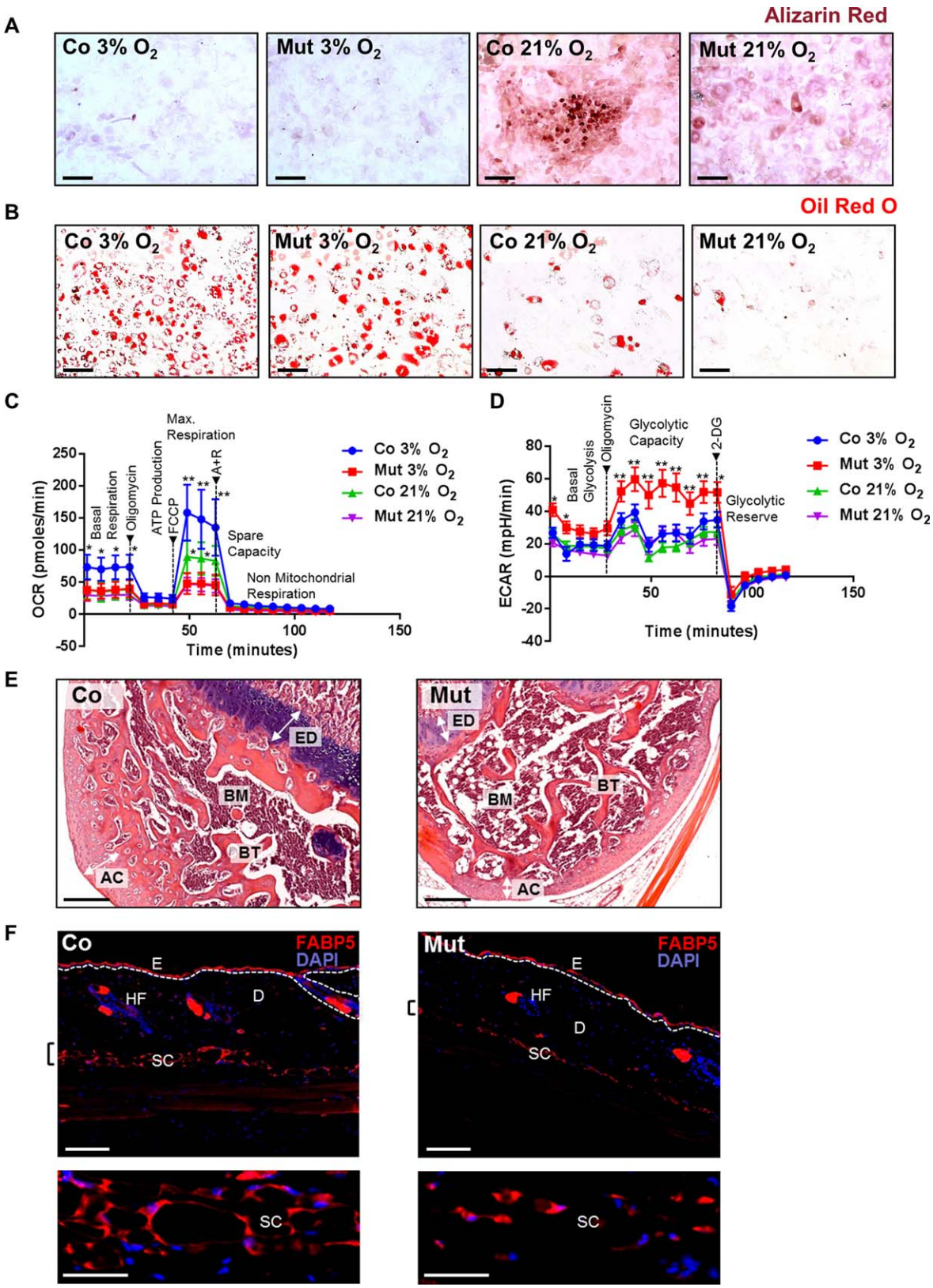

Figure 1. Impaired lineage differentiation and mitochondrial function in *Sod2*-deficient stromal precursor cells. **(A)**: Osteogenic differentiation is visualized by Alizarin red in co and mut precursors grown under 3% and 21% oxygen tension. Scale bars = 200 μm. **(B)**: Adipogenic differentiation is visualized by oil red O in co and mut precursors grown under 3% and 21% oxygen tension. Scale bars = 200 μm. **(C)**: Oxygen consumptionrate indicative of oxidative phosphorylation and **(D)** Extracellular acidification rate measurement indicative of glycolysis were performed under 3% and 21% oxygen conditions in co and mut precursors using real time flux analyzer. The data represent mean values of four technical replicates carried out three times, values were normalized to cell number. Error bars represent SEM values. *, $p < .05$; **, $p < .01$. **(E)**: Representative microphotographs of H&E stained sections of femur bone from co and mutant mice. Scale bars = 200 μm. **(F)**: Representative microphotographs with immunofluorescence staining for fatty acid binding protein 5 indicative of adipocytes in the skin from co and mut mice. Dashed line indicates the epidermal-dermal junction. Scale bars = 50 μm and for magnified view 20 μM. Abbreviations: AC, articular cartilage; BM, bone marrow; BT, bone trabeculae; co, new born control; D, dermis; DAPI, 4′,6-diamidino-2-phenylindole; E, epidermis; ECAR, extracellular acidification rate; ED, epiphyseal disk; FABP5, fatty acid binding protein 5; HF, hair follicle; mut, stroma-specific *Sod2*-deficient mice; OCR, oxygen consumption rate; SC, subcutaneous fat layer.

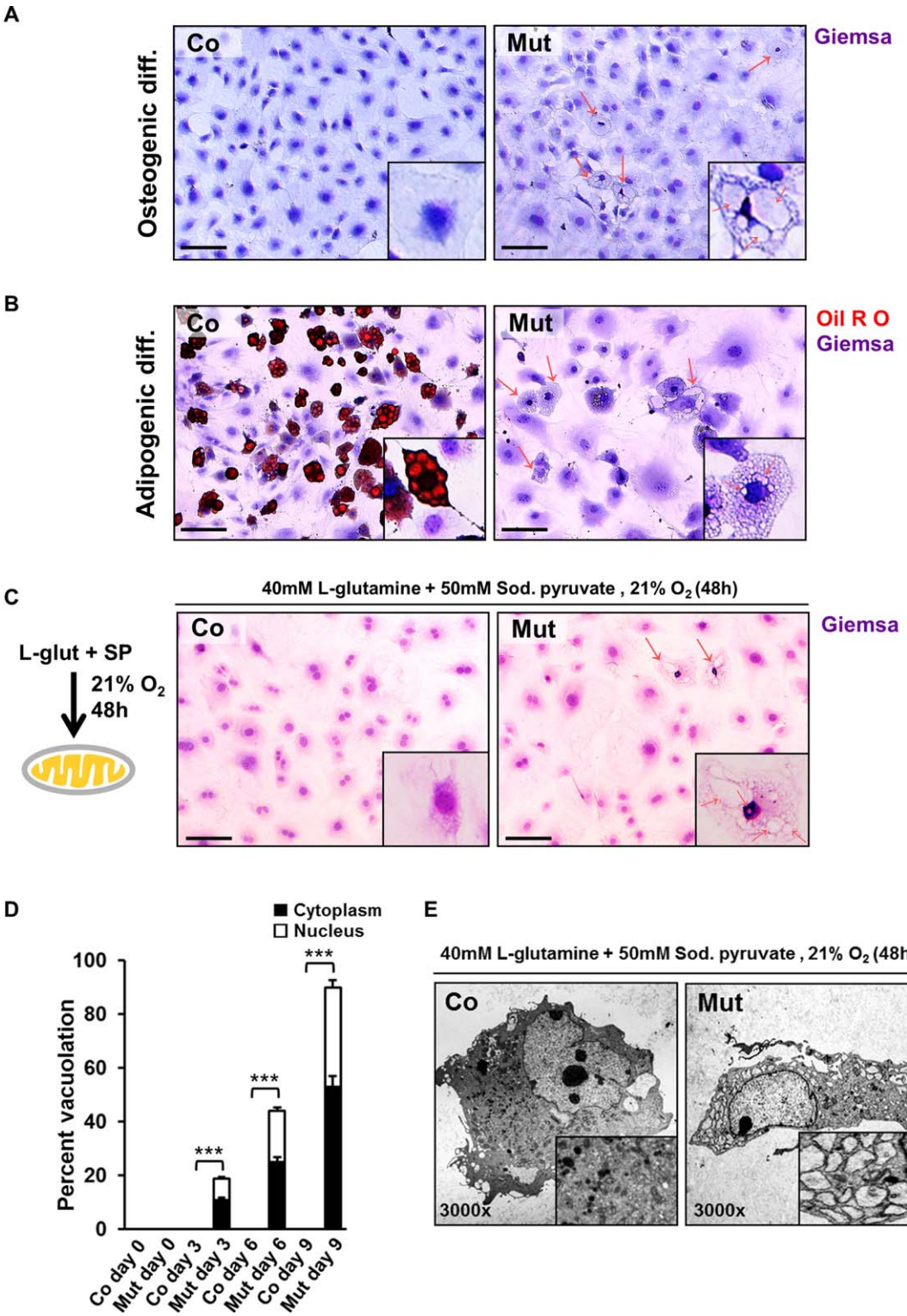

Figure 2. Enhanced nucleocytoplasmic vacuolation and chromatin condensation upon exposure to osteogenic, adipogenic induction media, and enforced oxidative metabolism in *Sod2*-deficient stromal precursors. **(A)**: Giemsa staining of osteogenic and **(B)** adipogenic differentiation following incubation of co and mut precursor cells with the corresponding induction media depict nucleocytoplasmic vacuolation in mut precursors. Scale bars = 200 μm. **(C)**: Giemsa staining of co and mut precursor cells after 48 hours and **(D)** quantification of nucleocytoplasmic vacuolation in mut and co stromal precursors following culture for the indicated period of time under forced oxidative metabolism conditions (40 mM L-glutamine [L-Glut] + 50 mM sodium pyruvate [SP], 21% O_2) without glucose. The values are presented as mean ± SEM of percentage vacuolation; respective comparisons are indicated with line and ***, $p < .001$. Scale bars = 200 μm. **(E)**: Transmission electron microscopic images show cell architecture in co and mut stromal precursors cultured under forced oxidative metabolism conditions (40 mM L-Glut + 50 mM SP, 21% O_2) without glucose. Note the vacuolation in mut cells as opposed to co cells, magnification 3,000×. Abbreviations: co, new born control; mut, stroma-specific *Sod2*-deficient mice; SP, sodium pyruvate.

cytoplasmic vacuolation in mut precursors substantially increased with time as opposed to wild type (Fig. 2D) and eventually lead to cell death within two weeks of culture. Electron microscopic further confirmed the presence of large vacuoles in mut precursors (Fig. 2E). Notably, these vacuoles were devoid of any cell organelle (Fig. 2E). However, when L-Glut or SP were used individually no nucleocytoplasmic vacuolation and subsequent cell death was observed (Supporting Information Fig. S3B). These data suggest that L-Glut and SP act synergistically to induce nucleocytoplasmic vacuolation, chromatin condensation, and cell death in mut precursors, which in consequence caused suppressed lineage differentiation of mut precursors.

Sod2-Deficient Stromal Precursors Revealed Global Metabolic Rearrangement

To gain insight into mechanisms driving metabolic dysregulation, we systematically analyzed the expression and activity of distinct key metabolic enzymes of glycolysis and TCA or citric acid cycle (Fig. 3A) in mut precursors with impaired mitochondria under standard culture conditions (25 mM D-glucose, 4 mM L-Glut, and no SP). Intriguingly, we found a significant increase in the expression of hypoxia-inducible factor-1alpha (Hif-1α), uncoupling protein 2 (UCP2) lactate dehydrogenase A (LDHA), and pyruvate dehydrogenase kinase 1 in mut precursors (Fig. 3B; Supporting Information Fig. S4A–S4D), proteins which have been implicated in the glycolytic shift [21, 22]. In addition, an increase in the phosphorylation of pyruvate dehydrogenase (PDH) was noticed in the mut precursors (Fig. 3B; Supporting Information Fig. S4E). Phosphorylation of PDH inhibits its enzymatic action and prevents conversion of pyruvate into acetyl-coA in the TCA cycle [23]. Strikingly, we observed a significant downregulation of the TCA enzymes SDH (Fig. 3B; Supporting Information Fig. S4F), which is located in mitochondria and serves a dual role in cellular metabolism.

Next, we sought to complementarily determine the activity of metabolic enzymes. Therefore, we analyzed different metabolites using LC-MS in co and mut precursors cultured under standard glucose conditions (25 mM D-glucose, 4 mM L-Glut, and no SP) at low- or high-oxygen tension. Heatmap analysis in conjunction with multivariate principal component analysis and volcano plot showed striking differences in several metabolites between co and mut precursors under low-oxygen conditions (Fig. 3C–3F). LC-MS analysis revealed higher abundance of TCA metabolites, amino acids, and glucose as well as enhanced lactate to pyruvate ratio in mut precursors under low-oxygen tension (Fig. 3C). At 21% O_2 conditions also, mut precursors displayed a similar pattern in TCA metabolites, lactate to pyruvate ratio, and amino acids (Fig. 3C). Top hits in unbiased pathway enrichment analysis in mut precursors under both low- and high-oxygen tension were "citric cycle (TCA cycle)," "alanine, aspartate, and glutamine," and "D-glutamine and D-glutamate metabolism" (Fig. 3G, 3H).

Collectively, these findings highlight a variety of adaptive escape mechanisms cells usually adopt to evade high mitochondrial ROS concentrations and toxic metabolites, which—if persisting—may have adverse consequences with impaired differentiation and enhanced cell death.

Glutamine and Pyruvate Metabolism Promotes Metabolic Catastrophe in *Sod2*-Deficient Stromal Precursors

To get more insight how oxidative metabolism impairs differentiation and enhance cell death in mut precursors, we next performed metabolite profiling under enforced TCA conditions (40 mM L-Glut + 50 mM SP, 21% O_2).

Surprisingly, metabolic profiling revealed a significant accumulation of TCA metabolites in mut precursors as opposed to co precursors under oxidative metabolism stimulating conditions (Fig. 4A–4D), indicating drastic alterations in metabolism. Pathway enrichment analysis revealed that citric cycle (TCA cycle) and alanine, aspartate, and glutamine were still among the top hits in mut precursors (Fig. 4E) similar to what we observed under normal glucose conditions. Interestingly, the magnitude of fold change in citric cycle (TCA cycle) was higher (20-fold) during enforced oxidative metabolism (Fig. 4E) compared with glycolysis condition in mut precursors both at 3% oxygen (10-fold) (Fig. 3G) and 21% oxygen (8-fold) (Fig. 3H). Strikingly, "pyruvate metabolism" was dramatically increased in mut precursors under enforced oxidative metabolism (Fig. 4E), which did not occur in pathway enrichment under glycolysis conditions at 3% oxygen (Fig. 3G) and at 21% oxygen (Fig. 3H). These results suggest that highly upregulated citric cycle (TCA cycle) and pyruvate metabolism accumulate toxic metabolites that impair differentiation in mut precursors.

Additionally, under enforced TCA conditions, we observed a severe loss of MMP (Fig. 5A) and a robust increase in $O_2^{\bullet-}$ concentration (Fig. 5B) in mut precursors compared with co precursors, while H_2O_2 concentration was decreased in mut precursors (Fig. 5C).

As a consequence, we detected enhanced DNA damage as indicated by increased γH2AX (Fig. 5D, 5E; Supporting Information Fig. S5A), a marker for DNA double strand breaks [24], and cleaved caspase-3 (indicator of apoptosis) expression (Fig. 5E) in mut precursors under enforced oxidative metabolic conditions. Notably, under persistent oxidative metabolism conditions, mut precursors switch to TCA cycle with enhanced pyruvate entry into mitochondria as indicated by activation of PDH (depicted by reduced phosphorylation), increased expression of SDH, and increased Hif-1α degradation (Fig. 5D; Supporting Information Fig. S5B–S5D). These finding are consistent with corresponding pathway enrichment analysis (Fig. 4E). Diminished MMP (Fig. 5A) and increased PDH activity (Fig. 5D; Supporting Information Fig. S5B) with a metabolic transformation to the TCA cycle under enforced oxidative conditions most likely push mut precursor cells into a profound metabolic crisis. Taken together, these results describe a metabolic catastrophe in mut precursors that become most obvious when conditions enforce cell dependence on mitochondrial oxidative metabolism. To the best of our knowledge, this phenomenon describing metabolic catastrophe as a leading cause for differentiation failure in mut precursors has previously not been reported.

Intrinsically Aged Stromal Precursors Revealed Several Overlapping Features with *Sod2*-Deficient Stromal Precursors Using Oxidative Metabolism

Aging is often associated with increased mitochondrial abnormalities [2, 3], which most likely alter both cellular metabolism and lineage differentiation. To test this hypothesis, we analyzed

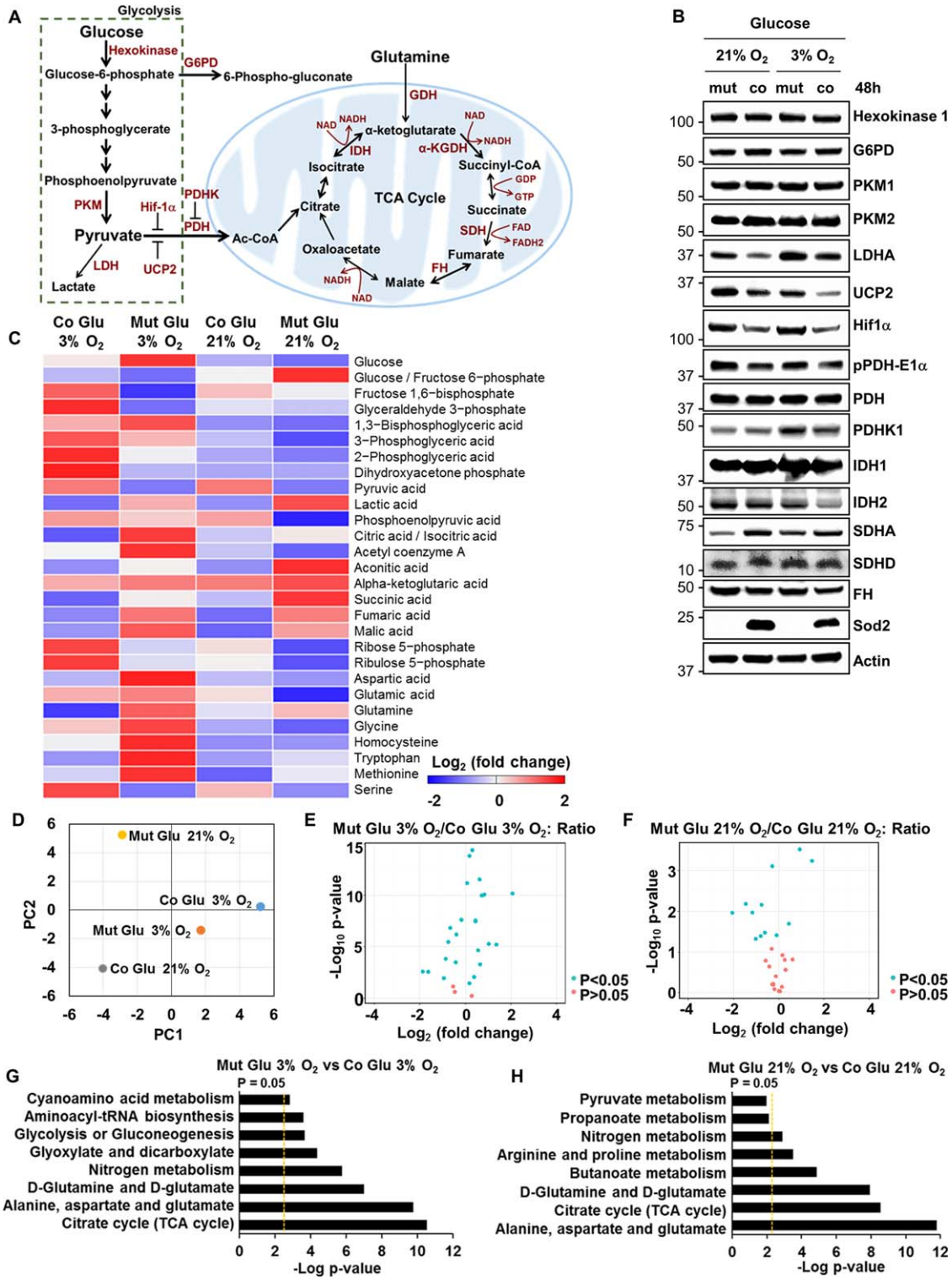

Figure 3. Altered cellular metabolism in mut precursors under both low- and high-oxygen tension. **(A)**: Schematic representation of integrated metabolic pathways including glycolysis and tricarboxylic acid (TCA) cycle. **(B)**: Western blot analysis with expression of different proteins involved in the glycolytic switch and metabolic enzymes participating in glycolysis and the TCA cycle. The Western blots are representative of three independent experiments. **(C)**: Heatmap depicting targeted metabolite profiling of samples ($n = 3$) from co and mut precursors cultured at 3% and 21% oxygen under standard glucose conditions (25 mM D-glucose, 4 mM L-glutamine, and no sodium pyruvate). The color reflects the log2 scale of relative metabolite concentration. **(D)**: Principal component analysis illustrating the variances between the different sample groups. Volcano plots showing the significantly changed metabolites (blue dots) at 3% oxygen **(E)** and **(F)** 21% oxygen tension. The integrated pathway analysis of metabolites displaying top enriched pathways in mut versus co at 3% oxygen **(G)** and 21% oxygen tension **(H)**. Dashed line represents *p* value of .05, which was considered significant for the over-represented pathways. Abbreviations: co, new born control; mut, stroma-specific *Sod2*-deficient mice; Glu, glutamine.

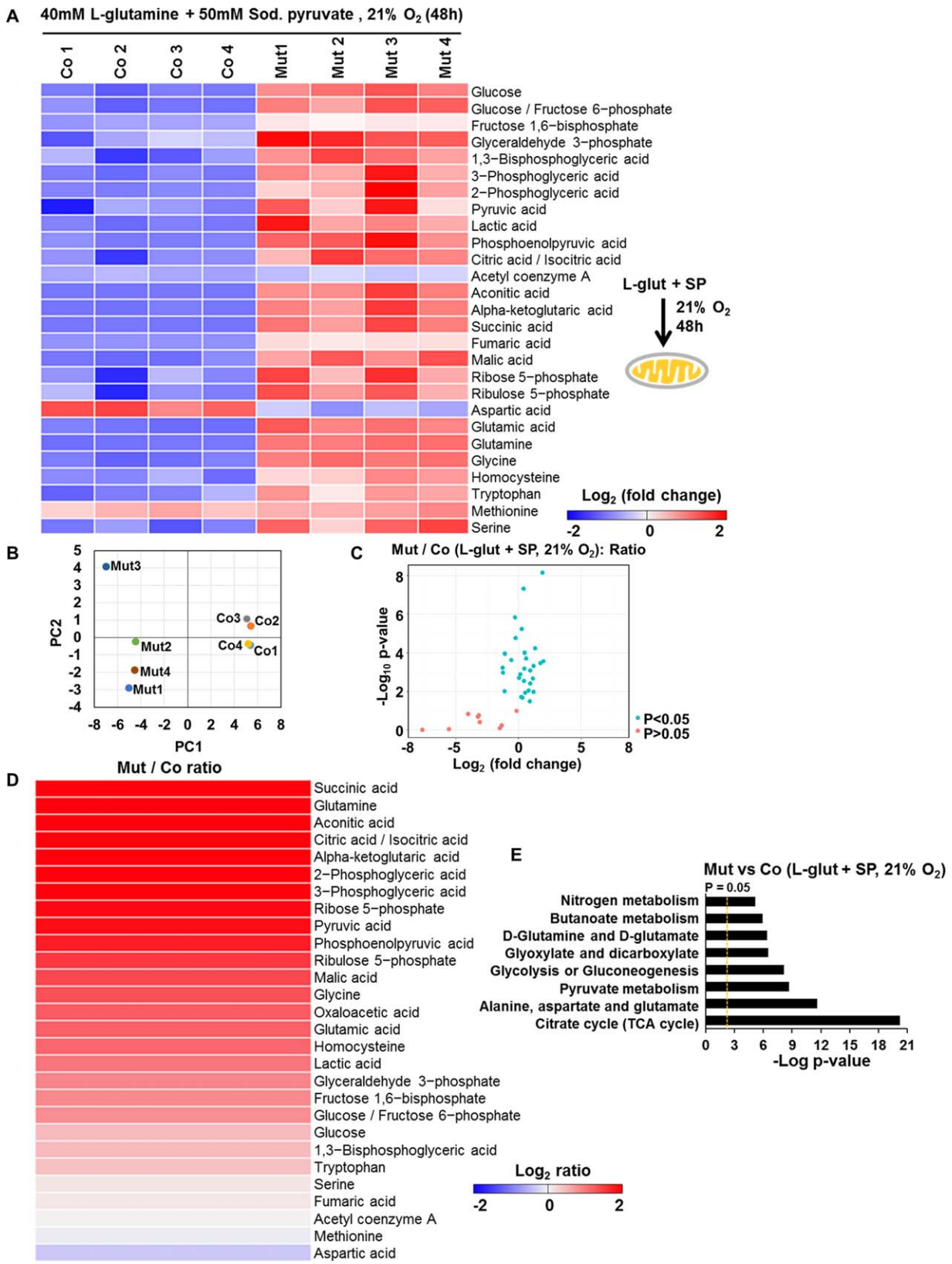

Figure 4. Persistent oxidative conditions force stromal precursor cells harboring defective mitochondria into metabolic crisis. **(A)**: Heatmap displaying relative abundance of metabolites extracted from co and mut precursors ($n = 4$ in each group) cultured for 48 hours under forced oxidative metabolism conditions (40 mM L-glutamine + 50 mM sodium pyruvate, 21% O_2) without glucose. Metabolites reveal consistent and significant alterations in abundance in the mut precursors using conditions of enforced oxidative metabolism. The color reflects the log2 scale. **(B)**: Principal component analysis (PCA) of the eight samples used to generate the heatmap in **(A)**. PCA was used to explore the quality of data and detect possible outliers. **(C)**: Significantly changed metabolites ($p < .05$) for each comparison are depicted in blue visualized by the volcano plots. **(D)**: Heatmap showing ratio of highly changed metabolites extracted from co and mut precursors under oxidative metabolism conditions. The color reflects the log2 scale. **(E)**: Integrated pathway analysis of metabolite displaying top enriched pathway in mut versus co during persistent oxidative metabolism. Dashed line represents p value of .05. $p < .05$ for the pathway enrichment was considered significant. Abbreviations: co, new born control; mut, stroma-specific *Sod2*-deficient mice.

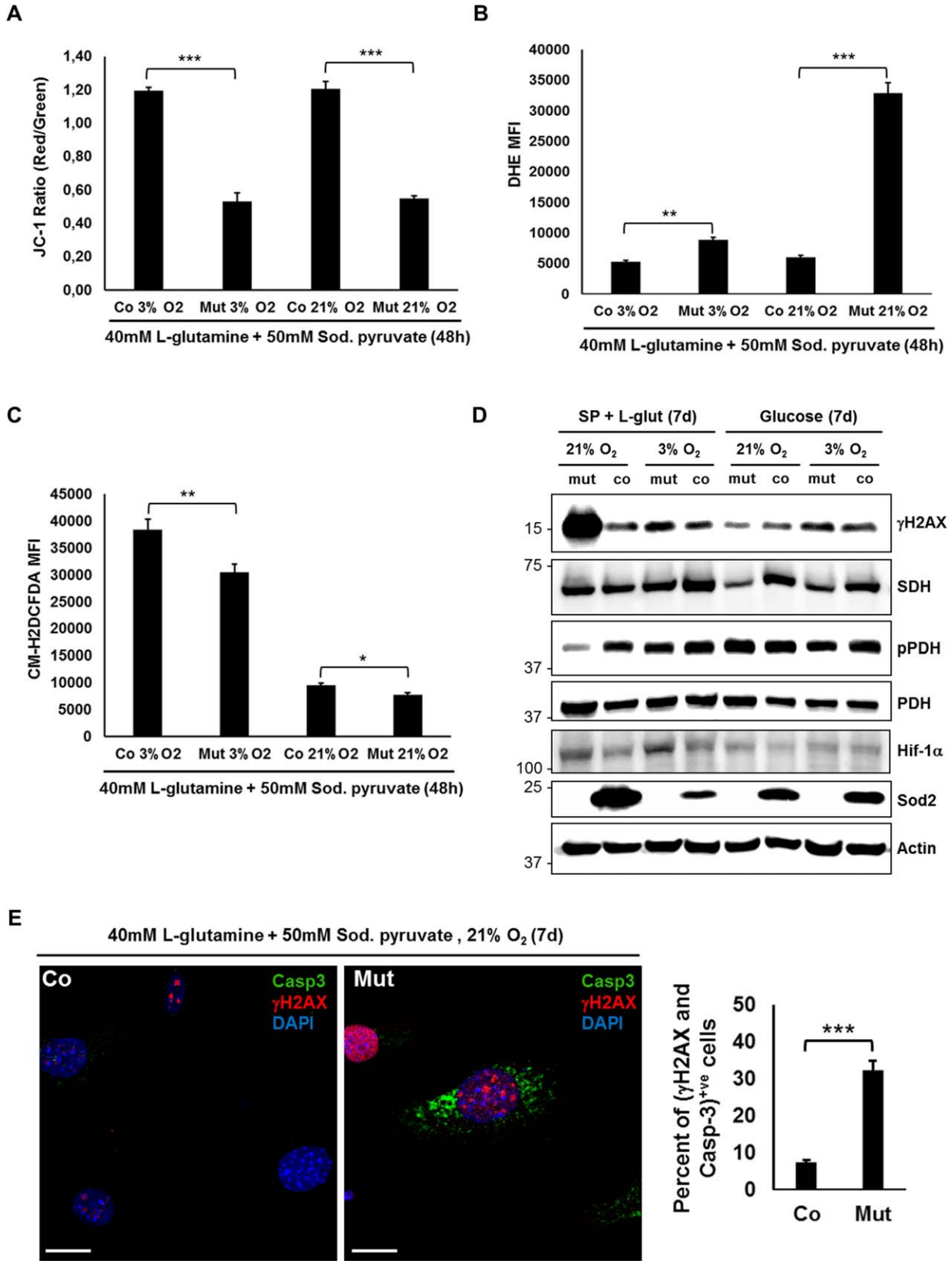

Figure 5. Persistent oxidative metabolism substantially enhances mitochondrial dysfunction and cellular damage in *Sod2*-deficient stromal precursors. **(A)**: Mitochondrial membrane potential was measured using JC-1 dye and JC-1 ratio was calculated. **(B, C)**: Reactive oxygen species were analyzed by dihydroethidium indicative of $O_2^{\bullet-}$ and CM-H2DCFDA predominantly indicative of H_2O_2. Representative graphs depict mean fluorescence intensities (MFI) normalized with unstained cells ($n = 3$). *, $p < .05$; **, $p < .01$ or ***, $p < .001$. **(D)**: Expression of indicated protein in co and mut precursor cells after 7 days at different culture conditions mimicking glycolysis and oxidative metabolism. The Western blots are representative of three independent experiments. **(E)**: Representative microphotographs with double immunofluorescence staining of γH2AX (red) and caspase-3 (green) and quantification in co and mut precursors cultured for 7 days under forced oxidative metabolism conditions (40 mM L-glutamine + 50 mM sodium pyruvate, 21% O_2) without glucose. 4′,6-diamidino-2-phenylindole (blue) was used to counterstain nuclei. The values are presented as percentage ± SEM; respective comparisons are indicated with line and, ***, $p < .001$ ($n = 3$). Scale bars = 20 μm. Abbreviations: co, new born control; DAPI, 4′,6-diamidino-2-phenylindole; DHE, dihydroethidium; JC-1, 5,5′,6,6′-tetrachloro-1,1′,3,3′-tetraethylbenzimidazolylcarbocyanine iodide; MFI, mean fluorescence intensities; mut, stroma-specific *Sod2*-deficient mice; SP, sodium pyruvate.

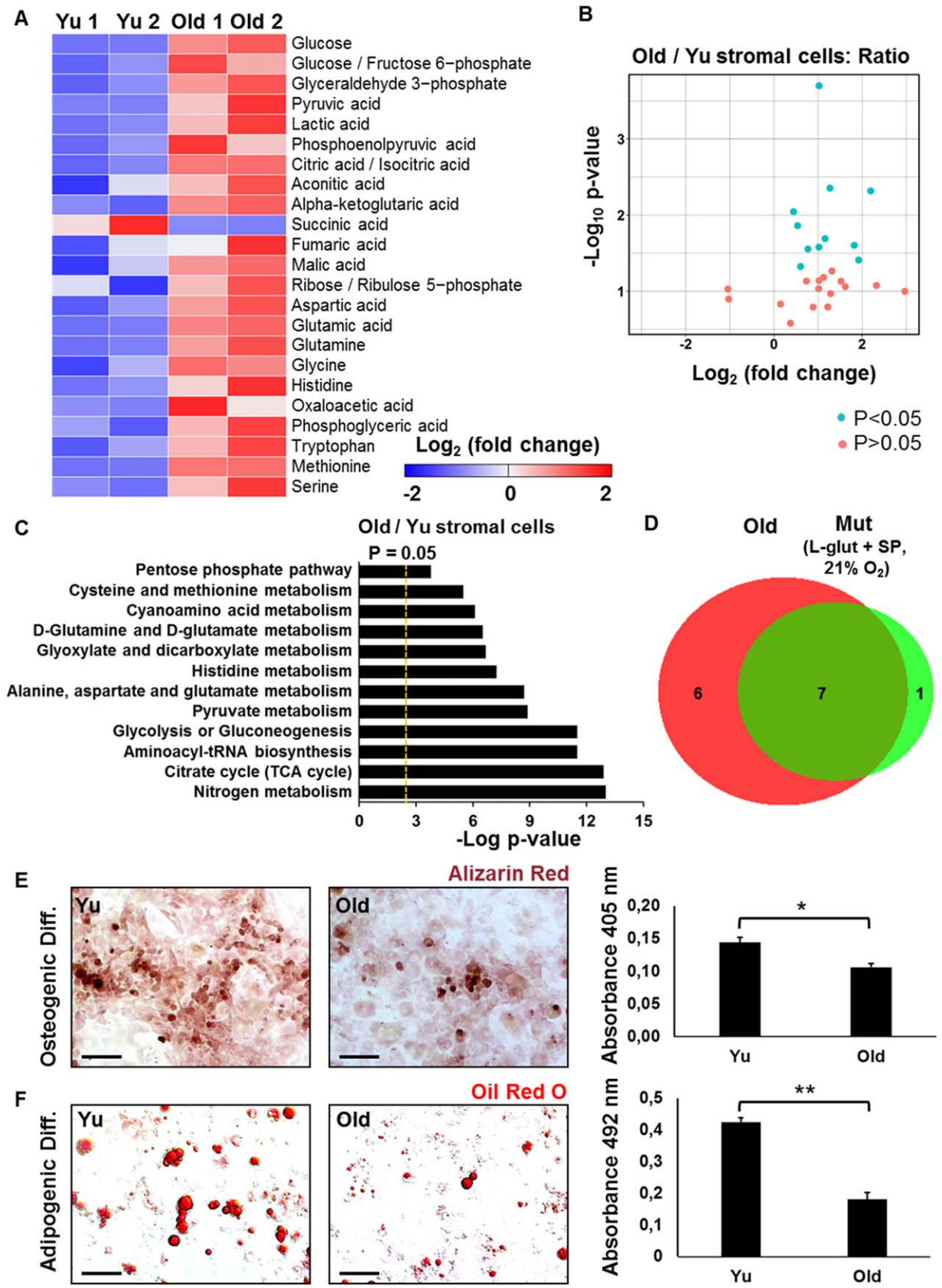

Figure 6. Enhanced oxidative metabolism results in impaired lineage differentiation of stromal cells during aging. **(A)**: Relative abundance of metabolites extracted from intrinsically young (Yu) and aged stromal cells isolated from 3 and 90 weeks aged mice, respectively. The color reflects the log2 scale. **(B)**: Volcano plot depicting significantly altered metabolites ($p < .05$) in blue between young and old stromal cells. **(C)**: Integrated pathway analysis of metabolite displaying top enriched pathway in old versus young. Dashed line represents p value of 0.05, which was considered significant for the overrepresented pathways. **(D)**: Venn diagram depicts substantial overlap of activated metabolic pathway between old stromal cells and mut precursors those were cultured under persistent oxidative conditions (40 mM L-glutamine + 50 mM sodium pyruvate, 21% O_2). **(E)**: Osteogenic differentiation is visualized and quantified by Alizarin red and **(F)** Adipogenic differentiation is visualized and quantified by oil red O in young and old stromal cells. Scale bars = 200 μm. *, $p < .05$; **, $p < .01$ ($n = 3$). Abbreviation: Mut, stroma-specific *Sod2*-deficient mice.

the changes in cellular metabolism and lineage differentiation among young and intrinsically old stromal cells freshly isolated from 3 and 90 weeks old mice, respectively.

Metabolic profiling revealed a substantial accumulation of TCA metabolites in intrinsically aged precursors as opposed to young precursors (Fig. 6A, 6B; Supporting Information Fig. S6A, S6B),

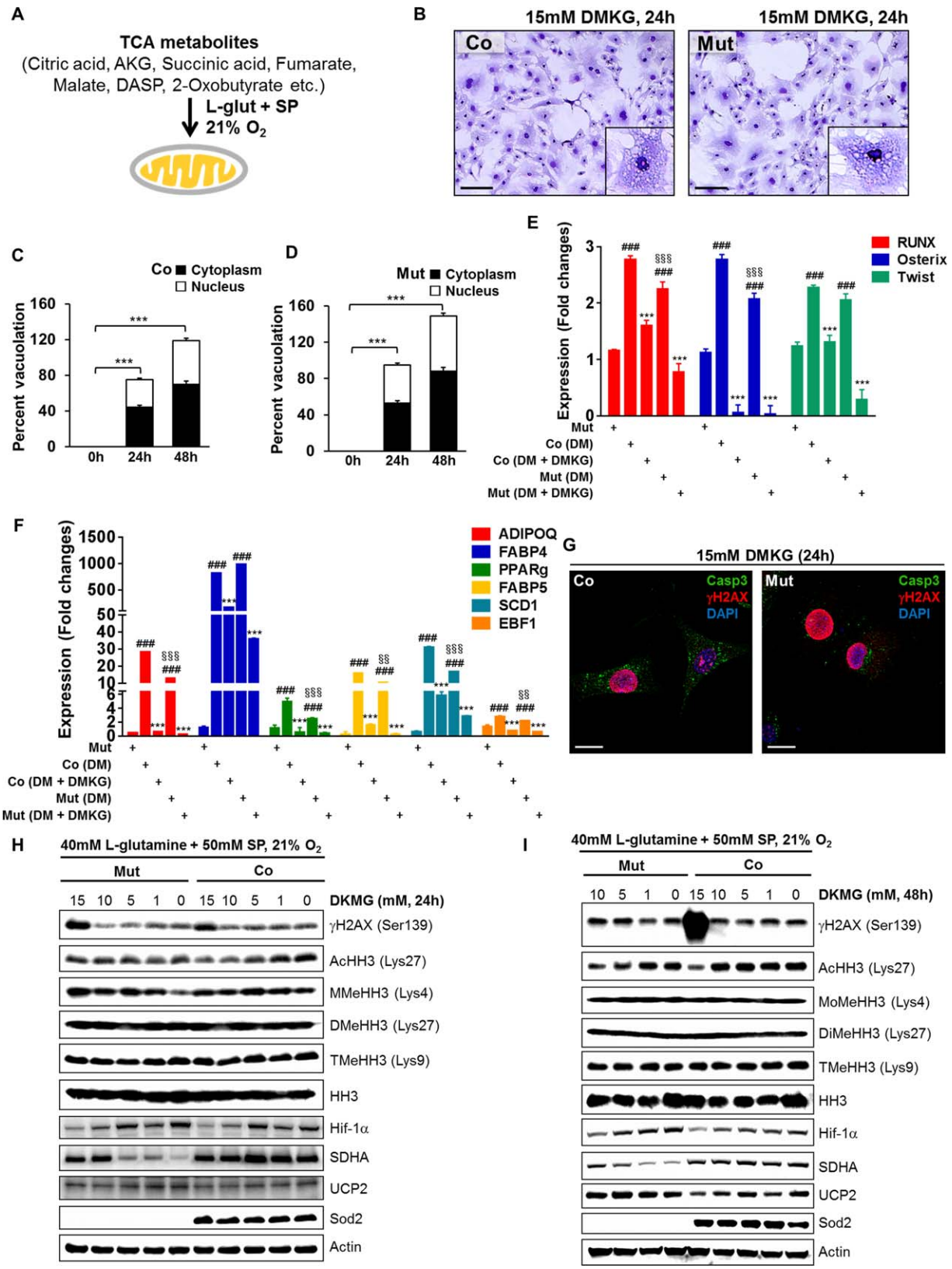

Figure 7.

suggesting considerable alterations in metabolism between young and old stromal precursors. Pathway enrichment analysis revealed that "nitrogen," citric cycle (TCA cycle), "Aminoacyl-tRNA biosynthesis," and "Pyruvate" metabolism were among the top hits in old as opposed to young stromal precursors (Fig. 6C). Interestingly, our analyses of activated metabolic pathway revealed striking overlap between intrinsically aged stromal cells and mut stromal cells those were cultured under enforced TCA conditions (40 mM L-Glut + 50 mM SP, 21% O_2) (Fig. 6D). In addition, the potential to undergo both osteo- and adipogenic differentiation were severely compromised in old compared with young stromal precursor cells (Fig. 6E, 6F). These results are consistent with earlier report [25–27] suggesting a severely impaired differentiation program during aging. In aggregate, these results provide evidence for the detrimental consequences of persistent oxidative metabolism on lineage differentiation of stromal cells.

Alpha-Ketoglutarate Triggers Cell Death via Induction of DNA Damage, Hif-1α Degradation, and Suppression of Histone H3 (Lys 27) Acetylation

To further dissect which intermediate/intermediates derived from oxidative metabolism of glutamine and pyruvate induces cell death in mut precursors, we exposed co and mut precursors to TCA metabolites that were highly enriched in mut precursor cells under conditions of persistent oxidative metabolism (Figs. 4D, 7A). Surprisingly, already after 24 hours of exposure with 15 mM dimethyl-α-ketoglutarate (DMKG), a cell-permeable derivative of α-ketoglutarate (AKG) [28], induction of nucleocytoplasmic vacuolation, and chromatin condensation in mut precursors was observed (Fig. 7B, 7D). Of note, at higher concentration, DMKG also induced nucleocytoplasmic vacuolation in co precursors (Fig. 7B, 7C), suggesting that DMKG at high concentrations is generally toxic and not specific to precursor cells with dysfunctional mitochondria. Direct exposure of 15 mM DMKG during osteo- and adipogenic differentiation for 48 hours significantly suppressed the expression of key genes involved in lineage differentiation both in co and mut precursors (Fig. 7E, 7F; Supporting Information Fig. S7A, S7B), indicating its opposing role on cell differentiation.

To gain more insight into the molecular mechanisms by which high abundance of AKG induces cell death through nucleocytoplasmic vacuolation in stromal precursors, we exposed co and mut precursors directly to DMKG. Interestingly, already after 24 hours, a significant increase in γH2AX expression both in co and mut precursors was observed (Fig. 7G, 7H; Supporting Information Fig. S8A, S8B). A higher extent of DNA damage leading to cell death within 48 hours was observed in the mut precursor cells (Fig. 7I; Supporting Information Fig. S9A). These data are consistent with our observation that excessive DNA damage occurred under conditions of enforced oxidative metabolism in mut precursor cells (Fig. 5D, 5E; Supporting Information Fig. S5A). In addition, DMKG significantly induced expression of cleaved caspase-3 both in co and mut stromal precursor cells, however, the magnitude was lower in mut (Fig. 7G) suggesting that cell death in mut may also involve non-apoptotic mechanisms. Together these data support the notion that AKG, an important TCA metabolite, does play a direct role in DNA damage and subsequent induction of cell death.

Recent studies have implicated AKG to be involved in epigenetic regulation [28, 29]. Stimulated by these studies, we explored whether AKG-mediated histone modification, in addition to γH2AX, is linked to nucleocytoplasmic vacuolation, chromatin condensation, cell death, and impaired differentiation. We did not identify any significant difference in histone methylation at different sites (Lys4, 9, and 27) after 24 and 48 hours exposure with DMKG (Fig. 7H, 7I). Strikingly, in case of histone acetylation, we found a significant decrease in acetyl histone H3 (Lys27) level after incubation with DMKG, and acetyl histone H3 (Lys27) suppression was more pronounced in mut precursors (Fig. 7H, 7I; Supporting Information Fig. S8C, S9B). Also, we observed reduced basal level of acetyl histone H3 (Lys27) in untreated mut when compared with untreated co precursors (Fig. 7H, 7I; Supporting Information Fig. S8C, S9B). This is most likely due to increased accumulation of AKG as a consequence of enhanced TCA cycle in mut precursors under enforced oxidative metabolism. The exact mechanism how AKG influence histone acetylation is currently unclear.

As AKG is also involved in the activation of various prolyl hydroxylases (PHD) family members [30], among them PHD1, 2, and 3 degrade Hif-1α—a key inducer of glycolysis—we wondered whether AKG also influences the stability of Hif-1α in stromal precursor cells. Interestingly, the cell permeable analogue of AKG, DMKG reduced the expression of Hif-1α but not UCP2 both in co and mut precursors in a dose-dependent manner (Fig. 7H, 7I; Supporting Information Fig. S8D, S9C). Of note, mut precursors displayed higher basal expression of

Figure 7. The cell-permeable AKG-derivative dimethyl-α-ketoglutarate (DMKG) directly promotes nucleocytoplasmic vacuolation through induction of DNA damage, Hif-1α degradation, and downregulation of acetylated histone H3 (Lys 27). **(A)**: Short sketch displaying the experimental setup. **(B)**: Giemsa staining of cells with visualization of vacuoles in the cytoplasm and in the nuclei and its quantification illustrating enhanced nucleocytoplasmic vacuolation both in co **(C)** and mut precursors **(D)** following exposure to 15 mM DMKG for 24 hours. The values are presented as mean ± SEM of percentage vacuolation; respective comparisons are indicated with line. ***, $p < .001$, ($n = 3$). Scale bars = 200 μm. **(E)**: Expression of indicated genes 48 hours after osteogenic differentiation and **(F)** adipogenic differentiation in co and mut stromal precursors in the presence and absence of 15 mM DMKG. ###, $p < .001$, (either co or mut without differentiation media vs. respective genotype of co or mut with differentiation media), ($n = 3$). ***, $p < .001$, (either co or mut with differentiation media vs. respective genotype of co or mut with differentiation media containing 15mM DMKG), ($n = 3$). §§, $p < .05$; §§§, $p < .001$, (co with differentiation media vs. mut with differentiation), ($n = 3$). The values of co without differentiation media are considered as onefold. DMKG: 15 mM DMKG. **(G)**: Representative microphotographs with double immunofluorescence staining of γH2AX (red) and caspase-3 (green) in the co and mut precursors exposed to 15 mM DMKG for 24 hours. 4′,6-Diamidino-2-phenylindole (blue) was used to counterstain nuclei. Scale bars = 20 μm. Expression of indicated protein in the co and mut precursors exposed to different concentrations of the cell permeable AKG analogue DMKG for 24 hours **(H)** and 48 hours **(I)**, highest dose (15 mM) of DMKG induced complete cell death in mut after 48 hours. The Western blots are representative of three independent experiments. Abbreviations: co, new born control; DM, differentiation media; DMKG, dimethyl-α-ketoglutarate; mut, stroma-specific *Sod2*-deficient mice; SP, sodium pyruvate.

Hif-1α compare with co cells in untreated groups (Fig. 7H, 7I; Supporting Information Fig. S8D, S9C). More importantly, DMKG induced the expression of SDH in mut precursors (Fig. 7H, 7I; Supporting Information Fig. S8E, S9D) that may reverse metabolism from glycolysis to oxidative metabolism and together with Hif-1α inhibition most likely induce metabolic catastrophe by over activating citric cycle (TCA cycle).

In conclusion, our results identify a profound metabolite imbalance in the mutant stromal precursors with faulty mitochondria affecting both glycolytic and oxidative metabolism. Metabolic catastrophe observed under oxidative metabolism conditions leads to accumulation of various TCA metabolites including AKG. Together these changes not only suppress the lineage differentiation but also promote nucleocytoplasmic vacuolation that eventually induce cell death.

Discussion

Mitochondria of differentiating stem and progenitors cells revamp significantly to meet the specific needs by altering their function, composition, structure, and maturation [31]. Here, we investigate how dysfunctional mitochondria modulates metabolic reprogramming and the fate of stromal or mesenchymal precursors undergoing differentiation using *Sod2*-deficient stromal precursor cells with accumulation of superoxide anions ($O_2^{\bullet -}$). This may be very relevant to organ aging, as both intrinsically aged human and mice reveal a profound increase in ROS and impairment of stroma rich organs eventually leading to atrophy of bone, adipose tissues, and skin.

Using the *Sod2*-deficient stromal precursor cells harboring functional and structural mitochondrial defects and intrinsically aged stromal cells, here, we identified substantial metabolic rearrangement, which together with high $O_2^{\bullet -}$ concentrations constitute the major cause for observed impairment of adipogenic and osteogenic lineage differentiation.

Enforced oxidative metabolism mimicking conditions of differentiating stem cells revealed dramatic dysregulation of citric acid cycle (TCA) and pyruvate metabolism in *Sod2*-deficient stromal precursors, we referred to as "metabolic catastrophe." Metabolic catastrophe is most likely a consequence of unrestricted entry of pyruvate due to the observed loss of MMP and increased activity of PDH. These findings are particularly important as oxidative metabolism plays a central role during osteogenic differentiation [20]. TCA cycle coupled to intact respiration, in fact induces the expression of osteocalcin, bone sialoprotein, osterix, and Runx2.[32] Similarly, increased OXPHOS activity and mitochondrial biogenesis has been detected during adipogenesis of mesenchymal stem cells, and a causal role for endogenous ROS at physiologic levels generated from respiratory complex III has been established [33].

In addition, we observed enhanced nucleocytoplasmic vacuolation and chromatin condensation during osteogenic and adipogenic differentiation that eventually drive cell death in mut stromal precursors. Our unbiased comprehensive screening approach identified AKG as a major culprit—accumulated during oxidative glutamine and pyruvate metabolism—that induces nucleocytoplasmic vacuolation, chromatin condensation, and cell death in mut precursor cells. Cell death induced by nucleocytoplasmic vacuolation in mut precursors under differentiating condition has previously not been described. Cytoplasmic vacuolation has earlier been implicated in cell death, such as myc-H-Ras and Rac-induced macropinocytosis or methuosis, while nuclei remained morphologically intact even in severely vacuolated and ruptured cells [34]. Notably, the cellular phenotype of nucleocytoplasmic vacuolation did not show the typical cell shrinkage and blebbing observed in apoptosis though display chromatin condensation [35].

Our data suggest that AKG accumulation involve distinct mechanisms in the induction of nucleocytoplasmic vacuolation, chromatin condensation, and in consequence cell death. First, AKG accumulation in mut precursors under persistent oxidative metabolic conditions directly induce DNA double strand breaks as indicated by an increase in γH2AX foci, and thereby activates DNA damage signaling. Enhanced DNA double strand breaks have been implicated in numerous disorders including aging [36, 37]. AKG-induced DNA damage—so far unreported in the literature—suppressed differentiation in mut precursors. Our findings underline the causal role of TCA metabolite in promoting DNA double strand breaks and this provides fresh insight into mechanisms underlying impaired differentiation in age-related disorders. Secondly, AKG strongly inhibited acetylation of histone H3 (Lys27) that marks active chromatin, acetylation of histone open chromatin and allows gene transcription. This finding is particularly relevant for adipocytes, as they require histone acetylation for transactivation of key metabolic proteins such as the glucose transporter glucose transporter 4 (GLUT4), hexokinase 2 (HK2), phosphofructokinase-1 (PFK1), lactate dehydrogenase A (LDHA), and the carbohydrate-responsive element binding protein, which are essential for the lipogenic programming [38]. In keeping with our finding that AKG inhibits acetylation of histone H3 (Lys27), the brown and white fat tissue size is severely reduced in stroma specific *Sod2* mutant mice. Thirdly, AKG abolished beneficial adaptive glycolysis and shift toward oxidative metabolism through enhancing SDH expression and by increasing Hif-1α degradation, making the condition even worse for mut precursors. AKG most likely exert its effect on Hif-1α degradation via activation of prolyl hydroxylases [30]. This notion is supported by earlier reports on increased Hif-1α activity and inhibition of the prolyl hydroxylase in the tumors harboring isocitrate dehydrogenase 1 (IDH1) and isocitrate dehydrogenase 2 (IDH2) mutations [39, 40]. Of note, AKG extended lifespan by inhibiting ATP synthase and target Of rapamycin (TOR) in healthy wild type cells [29]. AKG is involved in the maintenance of pluripotency state in embryonic stem cells multiple chromatin modifications [28]. Our results together with these reports establish a broader and multifaceted role for AKG as signaling molecule in addition to its metabolic function at physiological concentrations—if dysregulated—AKG may profoundly disturb tissue homeostasis.

Finally, it is evident that the aging process itself and virtually all age-related degenerative diseases are associated with secondary mitochondrial dysfunction and oxidative stress [37, 41]. Thus, our data are relevant to the understanding of disorders linked to abnormal mitochondria and enhanced ROS release in stromal precursors, which depend on intact TCA cycle and oxidative metabolism to differentiate into distinct lineages required for tissue homeostasis and regeneration. Therefore, restoring metabolite balance and limiting enhanced AKG levels either by its detoxification or by decreasing its synthesis may hold therapeutic potential for patients with mitochondrial dysfunction occurring during aging or even for mitochondrial disorders

associated with mutation in the α-ketoglutarate dehydrogenase complex [42]. Before therapeutically exploiting these strategies in clinical settings, additional in vitro and preclinical studies are needed to establish its causal role and efficacy.

Conclusion

Our study revealed persistent oxidative metabolism as a major reason for differentiation failure in stromal cells with mitochondrial dysfunction and in aged stromal cells. We identified excess accumulation of TCA cycle metabolite alpha-ketoglutarate in *Sod2*-deficient stromal precursors—due to metabolic rearrangement in response to increased mitochondrial ROS—as a major trigger for differentiation failure and cell death. The typical features of alpha-ketoglutarate-induced cell death include nucleocytoplasmic vacuolation and chromatin condensation. Mechanistically, we have shown that alpha-ketoglutarate execute cell death collectively through enhanced DNA damage, Hif-1α instability and reduced histone H3 acetylation (Lys27).

Acknowledgments

This work was supported by the German Research Foundation (DFG, SCHA411/15-2) within the Clinical Research Group KFO142 "Cellular and Molecular Mechanisms of Aging—From Mechanisms to Clinical Perspectives," the Graduate Training Centre GRK 1789 "Cellular and Molecular Mechanisms in Aging (CEMMA)," the Collaborative Research Center 1149 for trauma research at Ulm, and the Förderlinie Perspektivförderung "Zelluläre Entscheidungs- und Signalwege bei der Alterung" of the Ministerium für Wissenschaft, Forschung und Kunst Baden-Württemberg, Germany (to K.S.-K.). We thank Nicolas Schauer and Olivia Gräbner for metabolic profiling at the Metabolomic Discoveries GmbH, Potsdam, Germany.

Author Contributions

K.S.: conceived and designed the study, performed experiments and drafted the manuscript, read and approved the final manuscript; L.K., A.B., P.M., N.T., S.V.B.: technically supported this work, read and approved the final manuscript; M.W., S.K., W.B., H.G.: involved in designing and technically supporting the experiments, read and approved the final manuscript; P.M.: designed the experiments and involved in data analysis, read and approved the final manuscript; K.S.-K.: conceived and supervised the study and wrote the manuscript, read and approved the final manuscript.

Disclosure of Potential Conflicts of Interest

The authors indicate no potential conflicts of interest.

References

1 Wallace DC, Fan W, Procaccio V. Mitochondrial energetics and therapeutics. Annu Rev Pathol 2010;5:297–348.
2 Vafai SB, Mootha VK. Mitochondrial disorders as windows into an ancient organelle. Nature 2012;491:374–383.
3 Wang Y, Hekimi S. Mitochondrial dysfunction and longevity in animals: Untangling the knot. Science 2015;350:1204–1207.
4 Gomes AP, Price NL, Ling AJ et al. Declining NAD(+) induces a pseudohypoxic state disrupting nuclear-mitochondrial communication during aging. Cell 2013;155:1624–1638.
5 Lebovitz RM, Zhang H, Vogel H et al. Neurodegeneration, myocardial injury, and perinatal death in mitochondrial superoxide dismutase-deficient mice. Proc Natl Acad Sci USA 1996;93:9782–9787.
6 Li Y, Huang TT, Carlson EJ et al. Dilated cardiomyopathy and neonatal lethality in mutant mice lacking manganese superoxide dismutase. Nat Genet 1995;11:376–381.
7 Treiber N, Maity P, Singh K et al. Accelerated aging phenotype in mice with conditional deficiency for mitochondrial superoxide dismutase in the connective tissue. Aging Cell 2011;10:239–254.
8 Zhong W, Oberley LW, Oberley TD et al. Suppression of the malignant phenotype of human glioma cells by overexpression of manganese superoxide dismutase. Oncogene 1997;14:481–490.
9 Lunt SY, Vander Heiden MG. Aerobic glycolysis: Meeting the metabolic requirements of cell proliferation. Annu Rev Cell Dev Biol 2011;27:441–464.
10 Sullivan LB, Gui DY, Hosios AM et al. Supporting aspartate biosynthesis is an essential function of respiration in proliferating cells. Cell 2015;162:552–563.
11 Ryall JG, Cliff T, Dalton S et al. Metabolic reprogramming of stem cell epigenetics. Cell Stem Cell 2015;17:651–662.
12 Hart PC, Mao M, de Abreu AL et al. MnSOD upregulation sustains the Warburg effect via mitochondrial ROS and AMPK-dependent signalling in cancer. Nat Commun 2015;6:6053.
13 Sarsour EH, Kalen AL, Xiao Z et al. Manganese superoxide dismutase regulates a metabolic switch during the mammalian cell cycle. Cancer Res 2012;72:3807–3816.
14 Xu Y, Miriyala S, Fang F et al. Manganese superoxide dismutase deficiency triggers mitochondrial uncoupling and the Warburg effect. Oncogene 2015;34:4229–4237.
15 Ghesquiere B, Wong BW, Kuchnio A et al. Metabolism of stromal and immune cells in health and disease. Nature 2014;511:167–176.
16 Pattappa G, Heywood HK, de Bruijn JD et al. The metabolism of human mesenchymal stem cells during proliferation and differentiation. J Cell Physiol 2011;226:2562–2570.
17 Keating A. Mesenchymal stromal cells: New directions. Cell Stem Cell 2012;10:709–716.
18 Singh K, Maity P, Krug L et al. Superoxide anion radicals induce IGF-1 resistance through concomitant activation of PTP1B and PTEN. EMBO Mol Med. 20157:59–77.
19 Kim KH, Song MJ, Chung J et al. Hypoxia inhibits adipocyte differentiation in a HDAC-independent manner. Biochemical and Biophysical Research Communications 2005;333:1178–1184.
20 Shyh-Chang N, Daley GQ, Cantley LC. Stem cell metabolism in tissue development and aging. Development (Cambridge, England) 2013;140:2535–2547.
21 Zhang J, Khvorostov I, Hong JS et al. UCP2 regulates energy metabolism and differentiation potential of human pluripotent stem cells. Embo j 2011;30:4860–4873.
22 Requejo-Aguilar R, Lopez-Fabuel I, Fernandez E et al. PINK1 deficiency sustains cell proliferation by reprogramming glucose metabolism through HIF1. Nat Commun 2014;5:4514.
23 Kaplon J, Zheng L, Meissl K et al. A key role for mitochondrial gatekeeper pyruvate dehydrogenase in oncogene-induced senescence. Nature 2013;498:109–112.
24 Kuo LJ, Yang LX. Gamma-H2AX—A novel biomarker for DNA double-strand breaks. In Vivo (Athens, Greece) 2008;22:305–309.
25 Simic P, Zainabadi K, Bell E et al. SIRT1 regulates differentiation of mesenchymal stem cells by deacetylating beta-catenin. EMBO Mol Med 2013;5:430–440.
26 Chang HX, Yang L, Li Z et al. Age-related biological characterization of mesenchymal progenitor cells in human articular cartilage. Orthopedics 2011;34:e382–e388.
27 Connelly JT, Gautrot JE, Trappmann B et al. Actin and serum response factor transduce physical cues from the microenvironment to regulate epidermal stem cell fate decisions. Nat Cell Biol 2010;12:711–718.
28 Carey BW, Finley LW, Cross JR et al. Intracellular alpha-ketoglutarate maintains the pluripotency of embryonic stem cells. Nature 2015;518:413–416.
29 Chin RM, Fu X, Pai MY et al. The metabolite alpha-ketoglutarate extends lifespan by inhibiting ATP synthase and TOR. Nature 2014;510:397–401.
30 Wong BW, Kuchnio A, Bruning U et al. Emerging novel functions of the oxygen-

sensing prolyl hydroxylase domain enzymes. Trends Biochem Sci 2013;38:3–11.
31 Ito K Suda T. Metabolic requirements for the maintenance of self-renewing stem cells. Nat Rev Mol Cell Biol 2014;15:243–256.
32 D'ippolito G, Diabira S, Howard GA et al. Low oxygen tension inhibits osteogenic differentiation and enhances stemness of human MIAMI cells. Bone 2006;39:513–522.
33 Tormos KV, Anso E, Hamanaka RB et al. Mitochondrial complex III ROS regulate adipocyte differentiation. Cell Metab 2011;14:537–544.
34 Overmeyer JH, Kaul A, Johnson EE et al. Active ras triggers death in glioblastoma cells through hyperstimulation of macropinocytosis. Mol Cancer Res 2008;6:965–977.
35 Taylor RC, Cullen SP, Martin SJ. Apoptosis: Controlled demolition at the cellular level. Nat Rev Mol Cell Biol 2008;9:231–241.
36 Garinis GA, van der Horst GT, Vijg J et al. DNA damage and ageing: New-age ideas for an age-old problem. Nat Cell Biol 2008;10:1241–1247.
37 Lopez-Otin C, Blasco MA, Partridge L et al. The hallmarks of aging. Cell 2013;153: 1194–1217.
38 Wellen KE, Hatzivassiliou G, Sachdeva UM et al. ATP-citrate lyase links cellular metabolism to histone acetylation. Science 2009;324:1076–1080.
39 Lu C, Venneti S, Akalin A et al. Induction of sarcomas by mutant IDH2. Genes Dev 2013;27:1986–1998.
40 Zhao S, Lin Y, Xu W et al. Glioma-derived mutations in IDH1 dominantly inhibit IDH1 catalytic activity and induce HIF-1alpha. Science 2009;324:261–265.
41 Finkel T. The metabolic regulation of aging. Nat Med 2015;21:1416–1423.
42 Sheu KF, Blass JP. The alpha-ketoglutarate dehydrogenase complex. Ann NY Acad Sci 1999;893:61–78


See www.StemCells.com for supporting information available online.